

Alma Mater Studiorum Università di Bologna
Archivio istituzionale della ricerca

Mitochondrial Ca^{2+} -activated F1 FO -ATPase hydrolyzes ATP and promotes the permeability transition pore

This is the final peer-reviewed author's accepted manuscript (postprint) of the following publication:

Published Version:

Algieri, C., Trombetti, F., Pagliarani, A., Ventrella, V., Bernardini, C., Fabbri, M., et al. (2019). Mitochondrial Ca^{2+} -activated F1 FO -ATPase hydrolyzes ATP and promotes the permeability transition pore. ANNALS OF THE NEW YORK ACADEMY OF SCIENCES, 1457(1), 142-157 [10.1111/nyas.14218].

Availability:

This version is available at: <https://hdl.handle.net/11585/710352> since: 2019-12-22

Published:

DOI: <http://doi.org/10.1111/nyas.14218>

Terms of use:

Some rights reserved. The terms and conditions for the reuse of this version of the manuscript are specified in the publishing policy. For all terms of use and more information see the publisher's website.

This item was downloaded from IRIS Università di Bologna (<https://cris.unibo.it/>).
When citing, please refer to the published version.

(Article begins on next page)

This is the peer reviewed version of the following article:

C. Algieri, F. Trombetti, A. Pagliarani, V. Ventrella, C. Bernardini, M. Fabbri, M. Forni, S. Nesci (2019). Mitochondrial Ca^{2+} -activated F_1F_0 -ATPase hydrolyses ATP and promotes the permeability transition pore. *Annals of the New York Academy of Sciences*, 1457: 142-157.

which has been published in final form at <https://doi.org/10.1111/nyas.14218>.

This article may be used for non-commercial purposes in accordance with Wiley Terms and Conditions for Use of Self-Archived Versions.

1
2
3
4
5
6
7
8
9
10
11
12
13
14
15
16
17
18
19
20
21
22
23
24
25
26
27
28
29
30
31
32
33
34
35
36
37
38
39
40
41
42
43
44
45
46
47
48
49
50
51
52
53
54
55
56
57
58
59
60

The mitochondrial Ca^{2+} -activated $\text{F}_1\text{F}_\text{O}$ -ATPase hydrolyzes ATP and promotes the permeability transition pore

Cristina Algieri¹, Fabiana Trombetti¹, Alessandra Pagliarani^{1*}, Vittoria Ventrella¹, Chiara Bernardini¹, Micaela Fabbri¹, Monica Forni¹, Salvatore Nesci¹

¹ Department of Veterinary Medical Sciences; University of Bologna; Ozzano Emilia Via Tolara di Sopra 50, Bologna, 40064; Italy

*Corresponding author: alessandra.pagliarani@unibo.it

Short title: Mitochondrial Ca^{2+} - $\text{F}_1\text{F}_\text{O}$ -ATPase and the PTP

Keywords

Mitochondrial permeability transition pore, $\text{F}_1\text{F}_\text{O}$ -ATPase, inhibition kinetics, ATP hydrolysis, divalent cofactors, purified F_1 fraction.

Abstract

The properties of the mitochondrial F_1F_0 -ATPase catalytic site, which can bind Mg^{2+} , Mn^{2+} or Ca^{2+} and hydrolyses ATP, are explored by inhibition kinetic analyses to cast light on the Ca^{2+} -activated F_1F_0 -ATPase connection with the permeability transition pore (PTP), which initiates cascade events leading to cell death. While the natural cofactor Mg^{2+} activates the F_1F_0 -ATPase in competition with Mn^{2+} , Ca^{2+} is uncompetitive inhibitor in the presence of Mg^{2+} . Selective F_1 inhibitors, namely NBD-Cl, piceatannol, resveratrol and quercetin (Is- F_1), exert different mechanisms (mixed/uncompetitive inhibition) on the Ca^{2+} - or Mg^{2+} -activated F_1F_0 -ATPase, thus suggesting that the catalytic mechanism changes when Mg^{2+} is replaced by Ca^{2+} . In purified F_1 domain, the Ca^{2+} -activated F_1 -ATPase maintains the Is- F_1 sensitivity. The enzyme inhibition is accompanied by the maintenance of the mitochondrial calcium retention capacity and membrane potential. The data strengthen the Ca^{2+} -activated F_1F_0 -ATPase structural relationship with the PTP, in turn involved in physiological and pathological cellular changes.

Introduction

Mitochondria are now emerging as the core of vital and lethal cell events. Recently, the mitochondrial F_1F_0 -ATPase, the molecular engine embedded in the inner mitochondrial membrane (IMM), has been involved as key enzyme in the start of cascade events which lead to cell death. The molecular changes which would trigger the deathly mechanisms which stem from the IMM permeabilization are still a matter of debate and constitute a common feature both in pathological cells and in normal cells undergoing physiological modifications. The mitochondrial F_1F_0 -ATPase role in cell life is well known: the enzyme exploits the protonmotive force (Δp) across the IMM, generated by the respiratory complexes, to build ATP. The H^+ flux through the IMM-embedded F_0 domain, driven by Δp dissipation, rotates the enzyme rotor, which consists of the c -ring joined to the central stalk (ϵ , δ and γ subunit composition in mitochondria) ¹. The γ subunit protrudes in the hydrophilic- F_1 globular hexamer ($\alpha\beta$)₃ and transmits the rotation; in turn the torsion drives ATP synthesis by a binding change mechanism which involves three catalytic sites ² at the interface between α and β subunits of F_1 ³. Under pathophysiological conditions, when Δp becomes lower than Gibbs free energy of ATP hydrolysis, the enzyme acts in reverse, namely it rotates in the opposite direction, hydrolyzes ATP and re-energizes the IMM by pumping H^+ in the intermembrane space ⁴. The latter function is emerging as tightly linked to the cascade events associated with cell death.

Metal divalent cations can bind to the F_1F_0 -ATPase catalytic (β subunit) and non-catalytic (α subunit) sites in the different conformations ⁵. The asymmetry of the ($\alpha\beta$)₃ globular domain implies that the different conformational states of these sites imply different affinities for adenine nucleotides ⁶. The binding-change model is based on the peculiar structure of the F_1 domain, which hosts catalytic and non-catalytic sites. Three non-equivalent adenine nucleotide binding sites lie on the β subunit at the interface with α subunit, namely the open (empty) conformation β_E without nucleotides and the closed β_{DP} and β_{TP} states which bind Mg -ADP or Mg -ATP, respectively ². Conversely, the three equivalent adenine nucleotide binding sites on the non-catalytic α subunit occur in closed conformations at the α - β interface, *i.e.* α_E , α_{DP} and α_{TP} and only bind Mg -ATP ⁷ to remove ADP from the β_{DP} site and the related ADP-driven enzyme inhibition ^{8,9}. The natural cofactor Mg^{2+} allows ATP synthesis/hydrolysis and forms six coordination bonds in the catalytic site. Mg^{2+} can be replaced by other divalent cations, including Ca^{2+} ¹⁰. Ca^{2+} coordination geometry in the catalytic sites may lead to relevant conformational changes related to catalytic cooperativity. Accordingly, Ca^{2+} , which has bigger size than Mg^{2+} , can coordinate up to eight ligands, showing a less rigid geometry with irregular bond distances and angles ¹¹. The Ca^{2+} -activated F_1F_0 -ATPase is known to support ATP hydrolysis but not ATP synthesis. The F_1F_0 -ATPase in *Escherichia coli* hydrolyzes ATP in presence of Ca^{2+} and forms the pH gradient with nearly the same effectiveness as Mg^{2+} ¹². In bacteria ¹³, chloroplasts ¹⁴ and beef heart submitochondrial particles ¹⁰, the Ca^{2+} -activated F_1F_0 -ATPase was reported as unable to translocate H^+ . However, in swine heart

mitochondria the inhibition of the Ca^{2+} -activated F_1F_0 -ATPase by oligomycin and DCCD, both blockers of H^+ translocation within F_0 , is of the same extent as that of the Mg^{2+} -activated F_1F_0 -ATPase¹⁵. In inside-out submitochondrial particles the torque generation of the central stalk driven by Ca -ATP hydrolysis in F_1 ¹⁶ is coupled to the membrane F_0 sector and sensitive to the transmembrane electrochemical H^+ gradient¹⁵. Moreover, the failed mitochondrial ATP synthesis when the enzyme is stimulated by Ca^{2+} is associated with an increase in IMM permeability to ions and solutes and Δp disruption. The membrane permeation is ascribed to the formation and opening in the IMM of a regulated channel, known as permeability transition pore (PTP)^{17,18}. Up to now, Cyclophilin D (CypD) is the only identified positive modulator of PTP opening. Accordingly, CypD removal by cyclosporin A (CsA) inhibits the PTP¹⁹. The PTP is involved in some types of regulated cell death that feature severe human pathologies including cardiac/neurological ischemia, cancer and neurodegenerative diseases^{20,21}. Moreover, the PTP physiologically rules mitochondrial functions, cell differentiation and development²². The PTP nature and structural composition are still controversial, even if recent advances strongly support its origin from the F_1F_0 -ATPase^{23,24}. The Ca^{2+} coordination chemistry in the β subunits is consistent with PTP formation from the F_1F_0 -ATPase dimeric form²⁵. Ca^{2+} insertion would trigger conformational changes which would be transmitted from F_1 to the F_0 membrane subunits²⁶. Accordingly, changes in the IMM curvature would lead to disappearance of the *cristae*^{27,28} and to the formation of the PTP between the two detached F_0 monomers²⁹. To contribute to shoulder the hypothesis that the Ca^{2+} -ATP hydrolysis supported by the F_1F_0 -ATPase is required to open the PTP, the present work combines different biochemical strategies to enlighten the properties of the cation binding site when Ca^{2+} or Mg^{2+} are inserted and to investigate the impact of these cations on the enzyme catalytic mechanism.

Materials and methods

Chemicals

NBD-Cl (4-Chloro-7-nitro-1,2,3-benzoxadiazole) is obtained from Acros Organics. Resveratrol, Piceatannol, Cyclosporine A, JC-10, Fura-FF and Oligomycin were purchased by Vinci-Biochem (Vinci, Italy). Na_2ATP , Quercetin, Sodium succinate, Rotenone, Myxothiazol and FCCP (Carbonyl cyanide 4-(trifluoromethoxy)phenylhydrazone) were obtained from Sigma-Aldrich (Milan, Italy). All other chemicals were reagent grade. Quartz double distilled water was used for all reagent solutions except when differently stated.

Preparation of the mitochondrial fractions

Swine hearts (*Sus scrofa domestica*) were collected at a local abattoir and transported to the lab within 2 h in ice buckets at 0–4°C. After removal of fat and blood clots as much as possible, approximately 30–40 g of heart tissue were rinsed in ice-cold washing Tris-HCl buffer (medium A) consisting of 0.25 M sucrose, 10 mM Tris(hydroxymethyl)-aminomethane (Tris), pH 7.4 and finely chopped into fine pieces with scissors. Each preparation was made from one heart. Once rinsed, tissues were gently dried on blotting paper and weighted. Then tissues were homogenized in a buffer (medium B) consisting of 0.25 M sucrose, 10 mM Tris, 1 mM EDTA (free acid), 0.5 mg/mL BSA, pH 7.4 with HCl at a ratio of 10 mL medium B per 1 g of fresh tissue. After a preliminary gentle break up by Ultraturrax T25, the tissue was carefully homogenized by a motor-driven teflon pestle homogenizer (Braun Melsungen Type 853202) at 650 rpm with 3 up-and-down strokes. The mitochondrial fraction was then obtained by stepwise centrifugation (Sorvall RC2-B, rotor SS34). Briefly, the homogenate was centrifuged at 1,000 g for 5 min, thus yielding a supernatant and a pellet. The pellet was re-homogenized under the same conditions of the first homogenization and re-centrifuged at 1,000 g for 5 min. The gathered supernatants from these two centrifugations, filtered through four cotton gauze layers, were centrifuged at 10,500 g for 10 min to yield the raw mitochondrial pellet. The raw pellet was resuspended in medium A and further centrifuged at 10,500 g for 10 min to obtain the final mitochondrial pellet. The latter

was resuspended by gentle stirring using a Teflon Potter Elvehjem homogenizer in a small volume of medium A, thus obtaining a protein concentration of 30 mg/mL³⁰. All steps were carried out at 0–4°C. The protein concentration was determined according to the colorimetric method of Bradford³¹ by Bio-Rad Protein Assay kit II with bovine serum albumin (BSA) as standard. The mitochondrial preparations were then stored in liquid nitrogen until the evaluation of F-ATPase activities.

F₁ domain purification

Immediately after thawing, swine heart mitochondrial suspensions were diluted with 50 mL of medium A up to obtain a concentration of 20 mg/mL protein, sonicated on ice with MSE Soniprep 150 Sonicator at 210 μ m amplitude for 3 min for 3 times with 30 s intervals and centrifuged at 10,000 g for 10 min. The supernatant from this first centrifugation was further centrifuged at 100,000 g for 2 h. All these centrifugation steps were performed at 4°C. The pellet was resuspended in medium A plus 4 mM Na₂ATP, the pH adjusted to 9.2 by addition of small aliquots of 20% (w/w) NH₄OH solution and stored overnight at 4°C. Then the suspension, in which the pH was brought back to 8.0 by adding small aliquots of 2 N HCl aqueous solution, was sonicated at 210 μ m amplitude for 5 min. The sonicated suspension was centrifuged at 300,000 g for 1 h and the resulting pellet resuspended in 9 mL medium A plus 2 mM EDTA, pH 7.6. Then, after addition of 4.5 mL chloroform, the resulting dis-homogeneous mixture was vigorously vortexed for 15 and centrifuged at 600 g for 10 min to allow the separation of the two phases. The upper aqueous phase was collected and further centrifuged at 100,000 g for 1 h. The pale yellow supernatant obtained was supplemented with adequate aliquots of freshly prepared ATP solution to obtain a final concentration of 4 mM ATP and with 2N NaOH solution to adjust the pH to 8.0. After dropwise addition of saturated (NH₄)₂SO₄ solution plus 5 mM EDTA under continuous stirring to obtain 37% saturation and pH adjustment to 8.0 with 1N KOH solution, the suspension was centrifuged at 10,000 g for 15 min. The pellet was discarded and the collected supernatant was brought to 60% saturation with solid (NH₄)₂SO₄; the mixture was then adjusted to pH 8.0 with 1N KOH solution and kept overnight at 4°C. Finally, the pellet from the last centrifugation at 150,000 g for 90 min, resuspended by gentle stirring using a Teflon Potter Elvehjem homogenizer in a small volume of medium containing 100 mM TRIS/H₂SO₄, 1 mM EDTA and 50% glycerol, pH 8.0, constituted the purified F₁ fraction³². The protein concentration was determined according to the colorimetric method of Bradford³¹ by Bio-Rad Protein Assay kit II by using bovine serum albumin (BSA) as standard. The purified F₁ fraction was then stored in liquid nitrogen until the evaluation of F₁-ATPase activities.

Mitochondrial F-ATPase activity assays

Thawed mitochondrial preparations or purified F₁ fractions were immediately used for F-ATPase activity assays. The capability of ATP hydrolysis was assayed in a reaction medium (1 mL) containing 0.15 mg mitochondrial protein and 75 mM ethanolamine-HCl buffer pH 9.0, 6.0 mM Na₂ATP and 2.0 mM MgCl₂ for the Mg²⁺-activated F₁F₀-ATPase assay, and a the same buffer at pH 8.8 plus 3.0 mM Na₂ATP and 2.0 mM CaCl₂ for the Ca²⁺-activated F₁F₀-ATPase assay. After 5 min preincubation at 37°C, the reaction, carried out at the same temperature, was started by the addition of the substrate Na₂ATP and stopped after 5 min by the addition of 1 mL of ice-cold 15% (w/w) trichloroacetic acid aqueous solution. Once the reaction was stopped, vials were centrifuged for 15 min at 3,500 rpm (Eppendorf Centrifuge 5202). In the supernatant, the concentration of inorganic phosphate (Pi) hydrolyzed by known amounts of mitochondrial protein, which is an indirect measure of F-ATPase activity, was spectrophotometrically evaluated¹⁵. To this aim, 1 μ L from a mother solution of 3 mg/mL oligomycin in dimethylsulfoxide (DMSO) was directly added to the reaction mixture before starting the reaction. The total ATPase activity was calculated by detecting the Pi in control tubes run in parallel and containing 1 μ L DMSO per mL reaction system. In each experimental set, control tubes were alternated to the condition to be tested. The employed dose of oligomycin, specific inhibitor of F-ATPases which selectively blocks the F₀ subunit³³ ensured maximal enzyme activity inhibition and was currently used in F-ATPase assays. The F₁F₀-ATPase activity was routinely measured by subtracting, from

1
2
3
4
5
6
7
8
9
10
11
12
13
14
15
16
17
18
19
20
21
22
23
24
25
26
27
28
29
30
31
32
33
34
35
36
37
38
39
40
41
42
43
44
45
46
47
48
49
50
51
52
53
54
55
56
57
58
59
60

the P_i hydrolyzed by total ATPase activity, the P_i hydrolyzed in the presence of oligomycin ³⁴. In all experiments the F-ATPase activity was expressed as $\mu\text{mol } P_i \cdot \text{mg protein}^{-1} \cdot \text{min}^{-1}$.

Assay of F_1 -ATPase activity

Immediately after thawing, purified F_1 domains was immediately used for F_1 -ATPase activity assays. The capability of ATP hydrolysis was assayed in a reaction medium (1 mL) containing 0.15 mg F_1 purified protein and 75 mM ethanolamine-HCl buffer pH 9.0, 6.0 mM Na_2ATP and 2.0 mM MgCl_2 or 2.0 mM CaCl_2 for the Mg^{2+} -activated F_1F_0 -ATPase and Ca^{2+} -activated F_1F_0 -ATPase assay, respectively. The methods and parameters of ATP hydrolysis and P_i detection were the same as those used for “Mitochondrial F-ATPase activity assays”. The sensitivity to oligomycin was tested to verify the detachment of F_0 domain.

Kinetic analyses

To calculate the kinetic parameters (V_{\max} and K_m), enzyme activity data were fitted to the Michealis-Menten equation (1) in which the enzyme reaction rate (v), namely the F-ATPase activity, is plotted as a function of the concentration of substrate $[S]$. The mutual relationship between different metal cofactors and the ATP substrate (S) were also explored by building Hanes plots which follow equation (2), a rearrangement of Michaelis-Menten equation, in which the $[S]/v$ ratio is plotted against $[S]$. K_m and V_{\max} values were calculated from the intercept with x axis (changed to positive) and the reciprocal of the slope of the straight lines obtained, respectively. The IC_{50} values, namely the inhibitor concentration which causes half maximal inhibition of the enzyme activity, were calculated by fitting the enzyme activity data without inhibitor and in the presence of increasing inhibitor concentrations to the 4 parameter equation (3), in which the enzyme activity (y) is a function of the inhibitor concentration (i), “Range” is the difference between the maximal enzyme activity recorded (without inhibitor) and the residual enzyme activity which is not inhibited by any inhibitor concentration, defined as “Background”.

$$v = \frac{V_{\max} \cdot [S]}{K_m + [S]} \tag{1}$$

$$\frac{[S]}{v} = \frac{1}{V_{\max}}[S] + \frac{K_m}{V_{\max}} \tag{2}$$

$$y = \frac{\text{Range}}{1 + (\frac{x}{\text{IC}_{50}})^i} + \text{Background} \tag{3}$$

The graphical methods of Dixon and Cornish-Bowden plots, which complement one another ³⁵, were used to detect the inhibition mechanism of inhibitors of F_1 (Is-F_1) on the Ca^{2+} - or Mg^{2+} -activated F_1F_0 -ATPase. The reciprocal of the enzyme activity (Dixon plot) or the S/v ratio (Cornish-Bowden plot) were plotted as a function of the Is-F_1 concentration. To build these plots, different experimental sets were designed in which the F-ATPase activity was evaluated in the presence of increasing inhibitor concentrations at two concentrations of the Me^{2+} cofactor and constant ATP concentration or at two ATP concentrations, keeping the metal cofactor concentration constant. Therefore, in these experiments and plots alternatively the Me^{2+} cofactor or ATP played the S role. The values of K_i , which corresponds to the dissociation constant of the EI complex were calculated from the abscissa of the intercept of the straight lines obtained in the Dixon plots. The K'_i values, which represent the dissociation constant of the ternary ESI complex, were calculated by the abscissa of the intercept of the straight lines obtained in the Cornish-Bowden plots. In all plots the enzyme specific activity was taken as the expression of v . The correlation coefficients of all the straight lines obtained in Hanes, Dixon and Cornish Bowden plots were never lower than 0.95, thus confirming the linearity of these plots ³⁶. All data were processed by Grafit software (version 7.0.3).

SDS-PAGE and Western Blot assays

For SDS-PAGE assay, aliquots containing 5 µg of F₁ domain purified proteins were separated on Bolt 4–12% bis-Tris Plus (Life Technologies Ltd., Paisley, UK) for 55 min at 165 V. Upon the completion of electrophoresis, the gel was washed three times at ambient temperature with de-ionized water for 5 min each wash. The gels were then stained with SAFE BLUE (Coomassie blue) for 1 h with gentle shaking, and destained according to the manufacturer's instruction.

For Western Blot assay, SDS-PAGE separated proteins were electrophoretically transferred onto a nitrocellulose membrane by semidry Turbo Blot System (Bio-Rad Laboratories Inc., California, USA). The blot was washed in PBS and protein transfer was checked by staining the nitro-cellulose membranes with 0.2% Ponceau Red. Non-specific binding on nitrocellulose membranes was blocked with 5% milk powder in PBS-T20 (Phosphate Buffer Saline-0.1% Tween-20) for 1 h at room temperature. The membrane was then incubated over-night at 4°C with a 1:1000 dilution of Rabbit polyclonal anti-ATP5B Polyclonal Antibody (Aviva Systems Biology) in PBS-T20. After several washings with PBS-T20, the membrane was incubated with the secondary biotin-conjugate antibody (Goat Anti-Rabbit IgG Antibody) and then with a 1:1000 dilution of an anti-biotin horseradish peroxidase (HRP)-linked antibody. The western blot was developed using chemiluminescent substrate (Clarity Western ECL Substrate) according to the manufacturer's instructions. The intensity of the chemiluminescent signal of the resultant bands was acquired by a Fluor-ST Multimager using Quantity One Software (Bio-Rad Laboratories Inc., California, USA).

PTP and membrane potential evaluation

Swine heart mitochondria (1mg/mL) were suspended and energized in assay buffer (130 mM KCl, 1 mM KH₂PO₄, 20 mM HEPES, pH 7.2 con TRIS) incubated at 37°C with 1 µg/mL rotenone and 5 mM succinate as respiratory substrate. PTP opening was induced by the addition of small concentration of Ca²⁺ (20 µM) at fixed interval of time (1 min). The calcium retention capacity (CRC) was spectrofluorometrically evaluated in the presence of 0.5 µM Fura-FF. The probe has different spectral properties in the absence and in the presence of Ca²⁺, namely it displays excitation/emission spectra of 365/514 nm in the absence of calcium (Fura-FF low Ca²⁺) and shifts to 339/507 nm in the presence of high calcium concentrations (Fura-FF high Ca²⁺). PTP opening, which implies a decrease in CRC, was detected by the increase in fluorescence intensity ratio (Fura-FF high Ca²⁺)/(Fura-FF low Ca²⁺). The membrane potential (Δφ) was evaluated in presence of 0.5 µM JC-10. In polarized mitochondrial membranes, this probe selectively generates an orange JC-10 aggregate (excitation/emission spectra of 540/590 nm). The JC-10 monomers, generated when Δφ decreases, cause a green shift (excitation/emission spectra of 490/525 nm). Accordingly, the membrane depolarization (decrease in Δφ) ascribed to PTP formation was detected by the increase in the fluorescence intensity ratio which corresponds to an increased JC-10 aggregate/JC-10 monomers ratio. All measurements were processed by LabSolutions RF software.

Assay of the mitochondrial respiration

The frozen and thawed mitochondrial fractions were used to evaluate the mitochondrial respiration. The oxygen consumption rates were polarographically evaluated by Clark-type electrode using a thermostated Oxytherm System (Hansatech Instruments) equipped with a 1 mL polarographic chamber. The reaction mixture (120 mM KCl, 10 mM Tris-HCl buffer pH 7.2), maintained under Peltier thermostatisation at 37°C and continuous stirring, contained 0.25 mg mitochondrial protein. The succinate-O₂ oxidase activity by Complex II was determined by the oxidation of succinate in the presence of 1 µg/ml rotenone. The reaction was started by the addition of 10 mM succinate after 2 min of stabilization of oxygen signal and preliminary tests assessed that, under the conditions applied, succinate oxidation was suppressed by 1 µg/mL myxothiazol, selective inhibitor of complex III³⁷. The effect of succinate-O₂ oxidase activity was monitored at Is-F₁ concentrations corresponding to the IC₅₀ and at the concentration which induces the maximal inhibition of the Ca²⁺-activated

1
2
3
4
5
6
7
8
9
10
11
12
13
14
15
16
17
18
19
20
21
22
23
24
25
26
27
28
29
30
31
32
33
34
35
36
37
38
39
40
41
42
43
44
45
46
47
48
49
50
51
52
53
54
55
56
57
58
59
60

F₁F₀-ATPase. FCCP (0.1 μM) was added in order to verify the Is-F₁ effect on maximal mitochondrial respiratory activity. The rate of succinate-O₂ oxidase activities were monitored automatically by O₂view software as nmoles O₂·mg protein⁻¹·min⁻¹.

Quantification and Statistical Analysis

Statistical parameters including the number of replicates, dispersion and precision measures such as mean ± SD are reported in the figure legends. Data were subjected to one-way ANOVA followed by Dunnet’s test when *F* values indicated significance (*P* ≤ 0.05). The statistical analysis was performed using SigmaStat software (version 4).

Results

Divalent cations in the F₁F₀-ATPase kinetic mechanism of catalysis

In the presence of Mg²⁺, Mn²⁺ and Ca²⁺, the F₁F₀-ATPase supports ATP hydrolysis, even if with different efficiency. The ATPase activity sustained by Mg²⁺ or Mn²⁺ exhibit similar *V*_{max} and *K*_m values. Differently, the Ca²⁺-activated F₁F₀-ATPase shows a tenfold higher *K*_m value than the Mg²⁺-activated enzyme, while the *V*_{max} is approximately halved (Fig. 1A). These data are consistent with the reported values for Me²⁺ dependence of ATP hydrolysis in coupled submitochondrial particles¹⁰ and isolated F₁ domain³⁸. Therefore, kinetic analysis were carried out in the presence of Mg²⁺, Mn²⁺ and Ca²⁺ to obtain information on the mutual interactions between these cations. Mn²⁺ has an atomic radius similar to that of Mg²⁺ (1.61 Å Mn²⁺ Vs 1.45 Å Mg²⁺) and lower than that of Ca²⁺ (1.94 Å). Since the *K*_m of the Mg²⁺-activated F₁F₀-ATPase decreases as Mn²⁺ concentration increases, while the *V*_{max} is unaffected, the results indicate a competitive synergistic activation of Mn²⁺ with respect to Mg²⁺ (Fig. 1B), namely the two cations compete for the same site on the free enzyme. Conversely, Ca²⁺ in the reaction system of the Mg²⁺-activated F₁F₀-ATPases inhibits the F-ATPase activities by a non-competitive inhibition mechanism (the *V*_{max} decreases while the *K*_m is unaffected) (Fig. 1C). The non-competitive inhibition mechanism indicates that Ca²⁺ can bind either to the enzyme-MgATP complex or to the free enzyme.

Mechanism of F₁-ATPase inhibitors

Selective inhibitors of the catalytic F₁ domain (Is-F₁) can help to discriminate between the F₁F₀-ATPase response when ATP hydrolysis is sustained either by Mg²⁺ or by Ca²⁺. To this aim NBD-Cl (Fig. 2), piceatannol (Fig. 3), resveratrol (Fig. 4) and quercetin (Fig. 5) were tested under different experimental conditions, namely at different concentrations of ATP substrate and cation cofactor. The inhibition potency (estimated as IC₅₀ values) and kinetic mechanisms were investigated as reported in the Section “Kinetic analyses”.

NBD-Cl displays a higher inhibition efficiency on the Ca²⁺-activated F₁F₀-ATPase than on the Mg²⁺-activated F₁F₀-ATPase, as shown by the lower IC₅₀ value for the Ca²⁺-ATPase (Fig. 2A,F). Moreover, the Ca²⁺-activated F₁F₀-ATPase inhibition decreases when the ATP substrate or Ca²⁺ concentration are reduced (Fig. 2A). Conversely, the inhibition of the Mg²⁺-activated F₁F₀-ATPase only decreases when ATP concentration decreases (Fig. 2F). The inhibition exerted by NBD-Cl on both the Ca²⁺- and Mg²⁺-activated F₁F₀-ATPase shows uncompetitive mechanism with respect to the ATP substrate (Fig. 2B,C and G,H) and mixed type mechanism with respect to the cation cofactor (Fig. 2D,E and I,L). The uncompetitive inhibition indicates that the inhibitor only binds to the enzyme-ATP complex, while the mixed-type inhibition indicates that the inhibitor can also bind to the free enzyme. However, on considering the dissociation constants of the enzyme-inhibitor complex (*K*_i) and of the enzyme-substrate-inhibitor complex (*K*_i'), since both the Ca²⁺- and Mg²⁺-activated F₁F₀-ATPases show *K*_i values slightly lower than *K*_i' values, the formation of the binary complex

(enzyme-NBD) is preferred. Moreover, the K'_i values (Fig. 2C,H) are lower in the presence of Mg^{2+} than in the presence of Ca^{2+} , thus pointing out that NDB preferably binds to the Mg^{2+} -activated F_1F_0 -ATPase.

Piceatannol more efficiently inhibits the F_1F_0 -ATPase when activated by Ca^{2+} than when activated by Mg^{2+} . Moreover the inhibition kinetics reveals that the two differently activated F_1F_0 -ATPase activities show a different responsiveness to the inhibitor. The Ca^{2+} -activated F_1F_0 -ATPase inhibition is unaffected when the substrate or cofactor concentration decreases (Fig. 3A). In contrast, the Mg^{2+} -activated F_1F_0 -ATPase is less sensitive to piceatannol when ATP concentration decreases (Fig. 3F). Piceatannol exerts a mixed type inhibition mechanism on the Ca^{2+} -activated F_1F_0 -ATPase with respect to ATP substrate (Fig. 3B,C). The far lower K_i value with respect to the K'_i clearly indicates that the formation of the binary complex (enzyme-piceatannol) is favored with respect to that of the tertiary complex (enzyme-ATP-piceatannol). Piceatannol inhibition of the Ca^{2+} -activated F_1F_0 -ATPase is non-competitive with respect to Ca^{2+} (Fig. 3D,E). When the enzyme is activated by Mg^{2+} , piceatannol acts as uncompetitive inhibitor with respect to the ATP substrate (Fig. 3G,H). The plots drawn in Figure 3I,L clearly indicate a mixed-type inhibition mechanism with respect to Mg^{2+} , namely piceatannol can bind either to the free enzyme or to the enzyme- Mg^{2+} complex. Nevertheless, piceatannol binds to the Mg^{2+} -activated F_1F_0 -ATPase with nearly doubled affinity (halved K_i) to the free enzyme forming the enzyme-piceatannol complex rather than the ternary Mg^{2+} -enzyme-piceatannol complex (Fig. 3I,L). However, piceatannol more tightly binds to the Ca^{2+} -activated F_1F_0 -ATPase than to the Mg^{2+} -activated F_1F_0 -ATPase, as shown by the K_i and K'_i values for the Mg^{2+} -activated F_1F_0 -ATPase which are higher than those for the Ca^{2+} -activated F_1F_0 -ATPase. Moreover, the binding apparently depends on the cation cofactor concentration (Fig. 3A).

Resveratrol shows lower IC_{50} values for the Ca^{2+} -activated F_1F_0 -ATPase than for Mg^{2+} -activated F_1F_0 -ATPase. In both cases, the affinity for resveratrol decreases as the substrate concentration decreases (Fig. 4A,F). The inhibition of both the Ca^{2+} - and Mg^{2+} -activated F_1F_0 -ATPases is uncompetitive with respect to ATP (Fig. 4B,C and G,H) and the divalent cation (Fig. 4D,L and I,L). The K'_i values of the Ca^{2+} -activated F_1F_0 -ATPase with respect to ATP and cation cofactor are lower than those of the Mg^{2+} -activated F_1F_0 -ATPase. The data indicate that the uncompetitive inhibitor resveratrol more easily forms the tertiary complex (*i.e.* enzyme-substrate/cofactor-resveratrol) with the Ca^{2+} -activated F_1F_0 -ATPase than with the Mg^{2+} -activated ATPase.

Quercetin differently inhibits the Ca^{2+} - and Mg^{2+} -activated F_1F_0 -ATPases. The IC_{50} values of the Ca^{2+} -activated F_1F_0 -ATPase and Mg^{2+} -activated F_1F_0 -ATPase are unaffected by the substrate and/or cofactor concentrations (Fig. 5A,F). The inhibition mechanism exerted by quercetin on both the Ca^{2+} - and Mg^{2+} -activated F_1F_0 -ATPase activities is uncompetitive with respect to ATP (Fig. 5B,C and G,H) and the cofactors (Fig. 5D,E and I,L). However the K'_i value obtained for Ca^{2+} -activated F_1F_0 ATPase with respect to ATP (Fig. 5C) is approximately doubled with respect to that for the cation cofactor (Fig. 5E). Differently, in the case of the Mg^{2+} -activated F_1F_0 -ATPase the K'_i on ATP (Fig. 5H) and on the cofactor (Fig. 5L) attain similar values. Moreover, since the Ca^{2+} -activated F_1F_0 -ATPase shows lower IC_{50} and K'_i values for quercetin than the Mg^{2+} -activated F_1F_0 -ATPase, quercetin more tightly binds to the Ca^{2+} -activated F_1F_0 -ATPase than to the Mg^{2+} -activated F_1F_0 -ATPase.

The Ca^{2+} -dependent ATP hydrolysis by the F_1 domain is essential to open the PTP

The purified F_1 domain obtained from swine heart mitochondria and analyzed by SDS-PAGE, shows nine bands corresponding to the enzyme subunits (α , β , γ , δ , ϵ , b , OSCP, d and F6). The catalytic β subunit (MW 51,7KDa) was identified by Western blot analyses (Fig. 6A). Therefore the purified F_1 fraction contained the known subunits of the hydrophilic sector F_1 . In the purified swine F_1 domain the capability of ATP hydrolysis in the presence of either Mg^{2+} or Ca^{2+} and the sensitivity to F_1F_0 -ATPase inhibitors were tested. Other than $Is-F_1$, the selective inhibitor oligomycin was tested. Oligomycin blocks ATP synthesis/hydrolysis only when the membrane F_0 domain is functionally and structurally linked to F_1 portion³⁹. Accordingly, this macrolide antibiotic binds to two adjacent c subunits, covers the H^+ binding site and prevents the c -ring rotation⁴⁰. As in

the mitochondrial preparations (Fig. 1A), the F_1 -ATPase activity activated by Ca^{2+} (Fig. 6B) is lower than that activated by Mg^{2+} (Fig. 6C), even if the F_1 -ATPase/ F_1F_0 -ATPase activity ratio is higher when the F_1 -ATPase activity is sustained by Ca^{2+} than by Mg^{2+} (892.2 vs 644.2). Moreover, irrespective of the activating cation, the F_1 -ATPase activity is insensitive to oligomycin and inhibited by Is- F_1 (Fig. 6B,C), confirming that the purified fraction obtained only contains the F_1 domain detached from the membrane-embedded F_0 domain. Interestingly Ca^{2+} sustains ATP hydrolysis in the purified F_1 domain as in mitochondria.

When Ca^{2+} levels in mitochondria attain a threshold value, an uncontrolled Ca^{2+} release from mitochondria, associated with the collapse of the membrane potential ($\Delta\phi$), known as the electrical component of the Δp , occurs and the PTP opens^{41,42}. On considering these related events, PTP activity can be detected by adding Ca^{2+} and measuring changes in the calcium retention capacity (CRC) and $\Delta\phi$. The increase in CRC in control mitochondria, stimulated by subsequent 20 μM Ca^{2+} additions at fixed time intervals is abolished by CsA, a known PTP blocker. Similarly, PTP is inhibited by NBD-Cl, while the other F_1 inhibitors tested, namely piceatannol, resveratrol and quercetin, apparently desensitize PTP opening to Ca^{2+} (Fig. 7A). Accordingly, the increase in fluorescence intensity at Ca^{2+} pulses reveals that mitochondrial $\Delta\phi$ collapses, while both CsA and NBD-Cl prevent this event. Conversely, piceatannol and resveratrol apparently polarize the mitochondrial membrane. In the presence of quercetin, Ca^{2+} induce hormesis, namely initially it promotes an increase in fluorescence intensity, which would suggest $\Delta\phi$ collapse, while subsequent Ca^{2+} addition result in fluorescence intensity decrease, suggesting membrane repolarization (Fig. 7B).

Discussion

The combination of different experimental approaches lead to depict a quite realistic model of the intriguing and still poorly explored relationship between Ca^{2+} and PTP formation. Most likely, the F_1F_0 -ATPase catalytic sites undergo different conformational states, not only produced as illustrated by the binding-change mechanism², but also promoted by the binding of different cation cofactors, which lead to a different F -ATPase activation by the differently-sized divalent cations Mg^{2+} , Mn^{2+} and Ca^{2+} (Fig. 1A). The synergistic competitive activation of Mn^{2+} on the Mg^{2+} -activated F_1F_0 -ATPase is consistent with the enzyme- Me^{2+} complex formation, which can host either Mg^{2+} or Mn^{2+} during catalysis. In general, Me^{2+} -activated F_1F_0 -ATPases can sustain ATP hydrolysis, but especially Mg^{2+} - or Mn^{2+} -activated F_1F_0 -ATPases can link ATP hydrolysis to an efficient H^+ pumping activity¹⁰. On the other hand, the K_m and V_{max} values indicate that the Ca^{2+} -activated F_1F_0 -ATPase has lower catalytic efficiency than the Mg^{2+} -activated F_1F_0 -ATPase. The non-competitive inhibition of Ca^{2+} on the Mg^{2+} -activated F_1F_0 -ATPase suggests that Ca^{2+} and Mg^{2+} bind to distinct sites in the catalytic subunits of F_1 . Therefore, Ca^{2+} binds indifferently to the F_1F_0 -ATPase without cofactor or alternatively to the Mg^{2+} - F_1F_0 -ATPase, while Mg^{2+} and Mn^{2+} may bind to the same site which overlaps with that of Mg^{2+} (Fig. 1B,C). Mg^{2+} is known to form six bonds in the catalytic site of β subunits: one bond with the β Thr-163 of the P-loop (phosphate-binding loop), three bonds with the β Asp-256, β Glu-192 and β Arg-189 residues through three water molecules that build a bridge, and the last two bonds with the γ and β phosphate oxygens of ATP or ADP⁵. Most likely, the higher steric hindrance of Ca^{2+} with respect to Mg^{2+} and Mn^{2+} prevents its insertion in the catalytic sites with the hexa-coordinated geometry of Mg^{2+} ¹¹. Ca^{2+} would display a different coordination chemistry in the F_1 hexamer, promoting a spatial re-arrangement of the catalytic and non-catalytic sites, which can both bind divalent cations^{5,43}. Interestingly, within F_1 , the β Thr-163 is required to sustain the Ca^{2+} -dependent ATP hydrolysis and confers resistance to PTP opening^{13,25}.

The F_1 domain can bind covalent inhibitors which modify the aminoacid residues near the nucleotide-binding site in β subunits or non-covalent inhibitors, such as polyphenolic phytochemicals. To cast light on the catalytic mechanism, different inhibitor types were tested. NBD-Cl is a covalent inhibitor which mainly reacts with the β Tyr-311 and modifies its phenolic oxygen only when the catalytic site is in the β_E conformation⁴⁴. Moreover, the NBD group can move from Tyr to β Lys-162 of the P-loop within the same β_E subunit at pH ≥ 9.0 ⁴⁵. The NBD-Cl change occurs when the aminoacid residue is exposed at the α_E - β_E interface; the NBD group, by

making unfavourable steric clashes with the enzyme sidechain atoms, prevents the conversion to β_{TP} and blocks ATP hydrolysis⁴⁶ (Fig. S1). The similar inhibition mechanism exerted by NBD-Cl on the Ca^{2+} - and Mg^{2+} -activated F_1F_0 -ATPases with respect to cation cofactors or substrate (Fig. 2B,C-D,E and G,H-I,L) is consistent with the fact that the inhibitor does not occlude the nucleotide pocket. However, Ca^{2+} -binding to F_1 domain can favour the inhibitor interaction with the enzyme. Accordingly, conformational changes promoted by larger Ca^{2+} van der Waals radius with respect to Mg^{2+} which may make the binding site more prone to accommodate the inhibitor, are consistent with the more effective NBD-Cl inhibition with respect to the Mg^{2+} -activated F_1F_0 -ATPase (Fig. 2A,B). Polyphenolic phytochemicals, which abundantly occur in human diet, are known as beneficial in the treatment and prevention of human pathologies such as cancer and cardiovascular diseases (Bravo, 1998). Some of them (piceatannol, resveratrol and quercetin) inhibit ATP hydrolysis by F_1 without overlapping with the catalytic sites. They block the rotary mechanism by binding to individual and mutually independent sites in the hydrophobic region where the γ subunit C-terminal tip interacts with the “bearing”, a loops region below the “crown region” of α and β subunits⁴⁷ (Fig. S3). Consistently with their individual binding sites, piceatannol, resveratrol and quercetin exert different inhibition types on the Ca^{2+} - and Mg^{2+} -activated F_1F_0 -ATPases (Fig. 3,4,5). Furthermore, since their inhibition is never competitive under the different experimental conditions tested, each phytochemical binds to a distinct site from those of ATP, Mg^{2+} and Ca^{2+} . Consequently the latter, whose binding site is still unknown, most likely inserts in the nucleotide-binding pocket. Moreover, the phytochemical compounds inhibitory efficiency is always higher on the Ca^{2+} -activated F_1F_0 -ATPase than the Mg^{2+} -activated F_1F_0 -ATPase in all the tested conditions. Evidently, the Ca^{2+} size in the $(\alpha\beta)_3$ globular hexamer has a higher impact on the torsional mechanism of rotor. On considering that the inhibitory mechanism of piceatannol, resveratrol and quercetin acts on annular sleeve of the “bearing” by blocking the rotary mechanism driven by ATP hydrolysis, this loops region on the “nucleotide-binding domain” of β subunit may transmit the conformational change performed during enzyme catalysis through the “long connecting loop” to the “crown region” (Fig. S2). Indeed, molecular dynamics simulations suggest that the mechanical energy of Ca^{2+} insertion in β subunits is transmitted from the catalytic sites to the “crown region” and attains the OSCP subunit of the F_1F_0 -ATPase lateral stalk, which in turn transfers it to the IMM F_0 subunits leading to PTP opening^{25,26}. When, tested on the purified F_1 domain (Fig. 6A) detached from F_0 , the Is- F_1 confirmed their higher inhibition power on the Ca^{2+} -activated F_1F_0 -ATPase (Fig. 6B,C), even if ATP hydrolysis was still preferentially sustained by Mg^{2+} as in mitochondria. Thus, the Is- F_1 selectively inhibit the F_1 -ATPase activity and consequently the Ca^{2+} -dependent catalytic ATP hydrolysis mechanism of enzyme. Recent studies on the PTP, aiming at shedding light on the structural subunit(s) of F_1F_0 -ATPase involved in its formation, lead to two distinct hypothesis, namely the PTP would be formed by the c -ring or forms from F_1F_0 -ATPase dimers^{23,24,48–51}. However, the molecular mechanism which triggers PTP formation is still enigmatic²⁸. The Ca^{2+} -induced PTP opening is inhibited by CsA a known PTP blocker, in a similar way as by NBD-Cl (Figure 7A,B), while the polyphenolic phytochemicals increase the Ca^{2+} threshold required for PTP formation. Consistently, the $\Delta\phi$ decrease linked to PTP opening is similarly inhibited by CsA or by NBD-Cl, while the polyphenolic phytochemicals block the sudden $\Delta\phi$ dissipation due to PTP formation even though they affect the mitochondrial respiratory chain complex activities. Furthermore, in succinate-energized mitochondria the succinate- O_2 oxidase is activated by piceatannol and resveratrol and inhibited by quercetin, while NBD-Cl has no effect on mitochondrial respiration (Fig. S3).

The whole of data indicates that the differences between Mg^{2+} and Ca^{2+} in their coordination properties and the consequent adoption of different conformations within F_1 , even if not relevant to affect the catalytic mechanism of ATP hydrolysis, are functionally selective. Accordingly, only Ca^{2+} can drive the conformational transmission mechanism which leads to PTP opening.

On balance, Ca^{2+} promotes ATP hydrolysis by the mitochondrial F_1F_0 complex by a different kinetic mechanism from that of the natural cofactor Mg^{2+} , probably because of its bigger size and different chemical nature which prevent its insertion in the Mg^{2+} -site. However, Ca^{2+} binding close to the nucleotide site allows a conformational transmission mechanism which forms and opens the PTP. The model in which the F_1F_0 -ATPase is the key engine of cell life and death is strongly substantiated. When the Ca^{2+} concentration in mitochondria abruptly increases, the F_1F_0 -ATPase, known as the enzyme of life which synthesizes ATP, the universal energy currency molecule, binds Ca^{2+} and turns into an energy dissipation molecular engine, which

1
2
3
4
5
6
7
8
9
10
11
12
13
14
15
16
17
18
19
20
21
22
23
24
25
26
27
28
29
30
31
32
33
34
35
36
37
38
39
40
41
42
43
44
45
46
47
48
49
50
51
52
53
54
55
56
57
58
59
60

leads to cell death. The evidence that compounds targeting the F₁ domain inhibit both the Ca²⁺-dependent ATP hydrolysis and PTP opening suggests that the two mutually dependent cellular events are linked by a molecular mechanism. Since PTP opening is involved in a variety of physio-pathological events, the results stimulate research to discovery/design of selective drugs targeting the Ca²⁺-activated F₁F₀-ATPase to modulate the PTP.

Acknowledgments

Danilo Matteuzzi (Department of Veterinary Medical Sciences, University of Bologna) is gratefully acknowledged for kindly conferring swine hearts from a local abattoir to our lab. This work was supported by CARISBO Foundation grants to S.N. (2017/0313). C.A. and S.N. designed and conducted the experiments. C.B. performed gel electrophoresis and western blotting analysis. M.F. and M.F. contributed to experimental design. F.T., V.V., A.P. and S.N. conceived, designed, and directed the experiments. S.N. wrote the manuscript with assistance from A.P. and with input from all authors. The final version is approved by all authors. S.N. fund acquisition.

Competing interests

The authors declare no competing interests.

References

1. Kühlbrandt W. 2019. Structure and Mechanisms of F-Type ATP Synthases. *Annu. Rev. Biochem.*
2. Boyer P.D. 2002. Catalytic site occupancy during ATP synthase catalysis. *FEBS Lett.* **512**: 29–32.
3. Abrahams J.P., A.G. Leslie, R. Lutter, *et al.* 1994. Structure at 2.8 Å resolution of F₁-ATPase from bovine heart mitochondria. *Nature* **370**: 621–628.
4. Nicholls D.G. & S.J. Ferguson. 2013. 3 - Quantitative Bioenergetics: The Measurement of Driving Forces. In *Bioenergetics (Fourth Edition)* Nicholls D.G. & Ferguson S.J., Eds. 27–51. Boston: Academic Press.
5. Hahn A., K. Parey, M. Bublitz, *et al.* 2016. Structure of a Complete ATP Synthase Dimer Reveals the Molecular Basis of Inner Mitochondrial Membrane Morphology. *Mol. Cell* **63**: 445–456.
6. Frasch W.D. 2000. The participation of metals in the mechanism of the F(1)-ATPase. *Biochim. Biophys. Acta* **1458**: 310–325.
7. Hahn A., K. Parey, M. Bublitz, *et al.* 2016. Structure of a Complete ATP Synthase Dimer Reveals the Molecular Basis of Inner Mitochondrial Membrane Morphology. *Mol. Cell* **63**: 445–456.
8. Bald D., T. Amano, E. Muneyuki, *et al.* 1998. ATP synthesis by F₀F₁-ATP synthase independent of noncatalytic nucleotide binding sites and insensitive to azide inhibition. *J. Biol. Chem.* **273**: 865–870.
9. Weber J., C. Bowman, S. Wilke-Mounts, *et al.* 1995. alpha-Aspartate 261 is a key residue in noncatalytic sites of Escherichia coli F₁-ATPase. *J. Biol. Chem.* **270**: 21045–21049.
10. Papageorgiou S., A.B. Melandri & G. Solaini. 1998. Relevance of divalent cations to ATP-driven proton pumping in beef heart mitochondrial F₀F₁-ATPase. *J. Bioenerg. Biomembr.* **30**: 533–541.
11. Casadio R. & B.A. Melandri. 1996. CaATP inhibition of the MgATP-dependent proton pump (H⁺-ATPase) in bacterial photosynthetic membranes with a mechanism of alternative substrate inhibition. *Journal of Biological Inorganic Chemistry* **1**: 284–291.

12. Perlin D.S., L.R. Latchney, J.G. Wise, *et al.* 1984. Specificity of the proton adenosinetriphosphatase of *Escherichia coli* for adenine, guanine, and inosine nucleotides in catalysis and binding. *Biochemistry* **23**: 4998–5003.
13. Nathanson L. & Z. Gromet-Elhanan. 2000. Mutations in the β -subunit Thr159 and Glu184 of the *Rhodospirillum rubrum* F₀F₁ ATP synthase reveal differences in ligands for the coupled Mg²⁺- and decoupled Ca²⁺-dependent F₀F₁ activities. *Journal of Biological Chemistry* **275**: 901–905.
14. Pick U. & M. Weiss. 1988. A light-dependent dicyclohexylcarbodiimide-sensitive Ca-ATPase activity in chloroplasts which is not coupled to proton translocation. *Eur. J. Biochem.* **173**: 623–628.
15. Nesci S., F. Trombetti, V. Ventrella, *et al.* 2017. Kinetic properties of the mitochondrial F₁FO-ATPase activity elicited by Ca(2+) in replacement of Mg(2+). *Biochimie* **140**: 73–81.
16. Tucker W.C., A. Schwarz, T. Levine, *et al.* 2004. Observation of calcium-dependent unidirectional rotational motion in recombinant photosynthetic F₁-ATPase molecules. *J. Biol. Chem.* **279**: 47415–47418.
17. Hunter D.R. & R.A. Haworth. 1979. The Ca²⁺-induced membrane transition in mitochondria. III. Transitional Ca²⁺ release. *Arch. Biochem. Biophys.* **195**: 468–477.
18. Hunter D.R., R.A. Haworth & J.H. Southard. 1976. Relationship between configuration, function, and permeability in calcium-treated mitochondria. *J. Biol. Chem.* **251**: 5069–5077.
19. Baines C.P., R.A. Kaiser, N.H. Purcell, *et al.* 2005. Loss of cyclophilin D reveals a critical role for mitochondrial permeability transition in cell death. *Nature* **434**: 658–662.
20. Bernardi P., A. Rasola, M. Forte, *et al.* 2015. The Mitochondrial Permeability Transition Pore: Channel Formation by F-ATP Synthase, Integration in Signal Transduction, and Role in Pathophysiology. *Physiol. Rev.* **95**: 1111–1155.
21. Izzo V., J.M. Bravo-San Pedro, V. Sica, *et al.* 2016. Mitochondrial Permeability Transition: New Findings and Persisting Uncertainties. *Trends Cell Biol.* **26**: 655–667.
22. Pérez M.J. & R.A. Quintanilla. 2017. Development or disease: duality of the mitochondrial permeability transition pore. *Dev. Biol.* **426**: 1–7.
23. Bonora M., A. Bononi, E. De Marchi, *et al.* 2013. Role of the c subunit of the FO ATP synthase in mitochondrial permeability transition. *Cell Cycle* **12**: 674–683.
24. Giorgio V., S. von Stockum, M. Antoniel, *et al.* 2013. Dimers of mitochondrial ATP synthase form the permeability transition pore. *Proc. Natl. Acad. Sci. U.S.A.* **110**: 5887–5892.
25. Giorgio V., V. Burchell, M. Schiavone, *et al.* 2017. Ca(2+) binding to F-ATP synthase β subunit triggers the mitochondrial permeability transition. *EMBO Rep.* **18**: 1065–1076.
26. Nesci S., F. Trombetti, V. Ventrella, *et al.* 2018. From the Ca²⁺-activated F₁FO-ATPase to the mitochondrial permeability transition pore: an overview. *Biochimie* **152**: 85–93.
27. Baev A.Y., P.A. Elustondo, A. Negoda, *et al.* 2017. Osmotic regulation of the mitochondrial permeability transition pore investigated by light scattering, fluorescence and electron microscopy techniques. *Anal. Biochem.*
28. Nesci S. 2017. Mitochondrial permeability transition, F₁F₀-ATPase and calcium: an enigmatic triangle. *EMBO Rep* **18**: 1265–1267.
29. Nesci S. 2018. A Lethal Channel between the ATP Synthase Monomers. *Trends Biochem. Sci.* **43**: 311–313.
30. Nesci S., V. Ventrella, F. Trombetti, *et al.* 2016. Preferential nitrite inhibition of the mitochondrial F₁FO-ATPase activities when activated by Ca(2+) in replacement of the natural cofactor Mg(2+). *Biochim. Biophys. Acta* **1860**: 345–353.
31. Bradford M.M. 1976. A rapid and sensitive method for the quantitation of microgram quantities of protein utilizing the principle of protein-dye binding. *Anal. Biochem.* **72**: 248–254.
32. Penin F., C. Godinot & D.C. Gautheron. 1979. Optimization of the purification of mitochondrial F₁-adenosine triphosphatase. *Biochim. Biophys. Acta* **548**: 63–71.
33. Nicholls D.G. & S.J. Ferguson. 2013. 7 - ATP Synthases and Bacterial Flagella Rotary Motors. In *Bioenergetics (Fourth Edition)* 197–220. Boston: Academic Press.
34. Nesci S., V. Ventrella, F. Trombetti, *et al.* 2013. Mussel and mammalian ATP synthase share the same bioenergetic cost of ATP. *J. Bioenerg. Biomembr.* **45**: 289–300.

35. Cornish-Bowden A. 1974. A simple graphical method for determining the inhibition constants of mixed, uncompetitive and non-competitive inhibitors. *Biochem. J.* **137**: 143–144.
36. Nesci S., V. Ventrella, F. Trombetti, *et al.* 2011. Tributyltin (TBT) and dibutyltin (DBT) differently inhibit the mitochondrial Mg-ATPase activity in mussel digestive gland. *Toxicol In Vitro* **25**: 117–124.
37. Nesci S., F. Trombetti, M. Pirini, *et al.* 2016. Mercury and protein thiols: Stimulation of mitochondrial F1FO-ATPase and inhibition of respiration. *Chem. Biol. Interact.* **260**: 42–49.
38. Dorgan L.J., J.L. Urbauer & S.M. Schuster. 1984. Metal dependence and thermodynamic characteristics of the beef heart mitochondrial adenosine triphosphatase. *J. Biol. Chem.* **259**: 2816–2821.
39. Devenish R.J., M. Prescott, G.M. Boyle, *et al.* 2000. The Oligomycin Axis of Mitochondrial ATP Synthase: OSCP and the Proton Channel. *J Bioenerg Biomembr* **32**: 507–515.
40. Symersky J., D. Osowski, D.E. Walters, *et al.* 2012. Oligomycin frames a common drug-binding site in the ATP synthase. *Proc. Natl. Acad. Sci. U.S.A.* **109**: 13961–13965.
41. Haworth R.A. & D.R. Hunter. 1979. The Ca²⁺-induced membrane transition in mitochondria. II. Nature of the Ca²⁺ trigger site. *Arch. Biochem. Biophys.* **195**: 460–467.
42. Hunter D.R. & R.A. Haworth. 1979. The Ca²⁺-induced membrane transition in mitochondria. III. Transitional Ca²⁺ release. *Arch. Biochem. Biophys.* **195**: 468–477.
43. Hiller R. & C. Carmeli. 1985. Cooperativity among manganese-binding sites in the H⁺-ATPase of chloroplasts. *Journal of Biological Chemistry* **260**: 1614–1617.
44. Andrews W.W., F.C. Hill & W.S. Allison. 1984. Identification of the essential tyrosine residue in the beta subunit of bovine heart mitochondrial F1-ATPase that is modified by 7-chloro-4-nitro[14C]benzofurazan. *J. Biol. Chem.* **259**: 8219–8225.
45. Andrews W.W., F.C. Hill & W.S. Allison. 1984. Identification of the lysine residue to which the 4-nitrobenzofurazan group migrates after the bovine mitochondrial F1-ATPase is inactivated with 7-chloro-4-nitro[14C]benzofurazan. *J. Biol. Chem.* **259**: 14378–14382.
46. Orriss G.L., A.G. Leslie, K. Braig, *et al.* 1998. Bovine F1-ATPase covalently inhibited with 4-chloro-7-nitrobenzofurazan: the structure provides further support for a rotary catalytic mechanism. *Structure* **6**: 831–837.
47. Gledhill J.R., M.G. Montgomery, A.G.W. Leslie, *et al.* 2007. Mechanism of inhibition of bovine F1-ATPase by resveratrol and related polyphenols. *Proc. Natl. Acad. Sci. U.S.A.* **104**: 13632–13637.
48. Alavian K.N., G. Beutner, E. Lazrove, *et al.* 2014. An uncoupling channel within the c-subunit ring of the F1FO ATP synthase is the mitochondrial permeability transition pore. *Proc. Natl. Acad. Sci. U.S.A.* **111**: 10580–10585.
49. Carraro M., V. Checchetto, G. Sartori, *et al.* 2018. High-Conductance Channel Formation in Yeast Mitochondria is Mediated by F-ATP Synthase e and g Subunits. *Cell. Physiol. Biochem.* **50**: 1840–1855.
50. Guo L., M. Carraro, G. Sartori, *et al.* 2018. Arginine 107 of yeast ATP synthase subunit g mediates sensitivity of the mitochondrial permeability transition to phenylglyoxal. *J. Biol. Chem.* **293**: 14632–14645.
51. Neginskaya M.A., M.E. Solesio, E.V. Berezhnaya, *et al.* 2019. ATP Synthase C-Subunit-Deficient Mitochondria Have a Small Cyclosporine A-Sensitive Channel, but Lack the Permeability Transition Pore. *Cell Rep* **26**: 11-17.e2.

Figure Legends

Figure 1. Mitochondrial F_1F_0 -ATPase activities activated by divalent cations. A) Michealis-Menten plot of ATP hydrolysis sustained by Mn^{2+} , Mg^{2+} or Ca^{2+} . Hanes plots of the Mg^{2+} -activated F_1F_0 -ATPase activity in the absence (\square) or in the presence of 0.1 mM (\bullet) and 0.5 mM (\circ) Mn^{2+} (B); in the absence (\square) or in presence of 0.5 mM (\bullet) and 2.0 mM (\circ) Ca^{2+} (C). K_m and V_{max} are expressed in mM and $\mu\text{mol Pi}\cdot\text{mg protein}^{-1}\cdot\text{min}^{-1}$, respectively. Data represent the mean \pm SD from three independent experiments carried out on distinct mitochondrial preparations. Different letters indicate significantly different values within each treatment ($P \leq 0.05$).

Figure 2. NBD-Cl inhibition on the Ca^{2+} - (A-E) and Mg^{2+} -activated (F-L) F_1F_0 -ATPases. A) Dose-response curve at: 3 mM ATP + 2 (\square) or 0.5 mM Ca^{2+} (\bullet); 1 mM ATP + 2 mM Ca^{2+} (\circ). Dixon (B, D) and Cornish-Bowden (C, E) plots at 2 mM Ca^{2+} + 1 (\circ) or 3 mM ATP (\bullet); 3 mM ATP + 0.5 (\square) or 2 mM (\blacksquare) Ca^{2+} . (F) Dose-response curve at: 6 mM ATP + 2 (\square) or 0.5 mM Mg^{2+} (\bullet); 3 mM ATP + 2 mM Mg^{2+} (\circ). Dixon (G, I) and Cornish-Bowden (H, L) plots at 2 mM Mg^{2+} + 3 (\circ) or 6 mM ATP (\bullet); 6 mM ATP + 0.5 (\square) or 2 mM Mg^{2+} (\blacksquare). K_i and K'_i values were obtained as detailed in the Kinetic analyses section. Each point represents the mean \pm SD from three experiments on distinct mitochondrial preparations. Different letters indicate significant differences ($P \leq 0.05$).

Figure 3. Piceatannol inhibition on the Ca^{2+} - (A-E) and Mg^{2+} -activated (F-L) F_1F_0 -ATPases. A) Dose-response curve at: 3 mM ATP + 2 (\square) or 0.5 mM Ca^{2+} (\bullet); 1 mM ATP + 2 mM Ca^{2+} (\circ). Dixon (B, D) and Cornish-Bowden (C, E) plots at 2 mM Ca^{2+} + 1 (\circ) or 3 mM ATP (\bullet); 3 mM ATP + 0.5 (\square) or 2 mM (\blacksquare) Ca^{2+} . (F) Dose-response curve at: 6 mM ATP + 2 (\square) or 0.5 mM Mg^{2+} (\bullet); 3 mM ATP + 2 mM Mg^{2+} (\circ). Dixon (G, I) and Cornish-Bowden (H, L) plots at 2 mM Mg^{2+} + 3 (\circ) or 6 mM ATP (\bullet); 6 mM ATP + 0.5 (\square) or 2 mM Mg^{2+} (\blacksquare). K_i and K'_i values were obtained as detailed in the Kinetic analyses section. Each point represents the mean \pm SD from three experiments on distinct mitochondrial preparations. Different letters indicate significant differences ($P \leq 0.05$).

Figure 4. Resveratrol inhibition on the Ca^{2+} - (A-E) and Mg^{2+} -activated (F-L) F_1F_0 -ATPases. A) Dose-response curve at: 3 mM ATP + 2 (\square) or 0.5 mM Ca^{2+} (\bullet); 1 mM ATP + 2 mM Ca^{2+} (\circ). Dixon (B, D) and Cornish-Bowden (C, E) plots at 2 mM Ca^{2+} + 1 (\circ) or 3 mM ATP (\bullet); 3 mM ATP + 0.5 (\square) or 2 mM (\blacksquare) Ca^{2+} . (F) Dose-response curve at: 6 mM ATP + 2 (\square) or 0.5 mM Mg^{2+} (\bullet); 3 mM ATP + 2 mM Mg^{2+} (\circ). Dixon (G, I) and Cornish-Bowden (H, L) plots at 2 mM Mg^{2+} + 3 (\circ) or 6 mM ATP (\bullet); 6 mM ATP + 0.5 (\square) or 2 mM Mg^{2+} (\blacksquare). K_i and K'_i values were obtained as detailed in the Kinetic analyses section. Each point represents the mean \pm SD from three experiments on distinct mitochondrial preparations. Different letters indicate significant differences ($P \leq 0.05$).

Figure 5. Quercetin inhibition on the Ca^{2+} - (A-E) and Mg^{2+} -activated (F-L) F_1F_0 -ATPases. A) Dose-response curve at: 3 mM ATP + 2 (\square) or 0.5 mM Ca^{2+} (\bullet); 1 mM ATP + 2 mM Ca^{2+} (\circ). Dixon (B, D) and Cornish-Bowden (C, E) plots at 2 mM Ca^{2+} + 1 (\circ) or 3 mM ATP (\bullet); 3 mM ATP + 0.5 (\square) or 2 mM (\blacksquare) Ca^{2+} . (F) Dose-response curve at: 6 mM ATP + 2 (\square) or 0.5 mM Mg^{2+} (\bullet); 3 mM ATP + 2 mM Mg^{2+} (\circ). Dixon (G, I) and Cornish-Bowden (H, L) plots at 2 mM Mg^{2+} + 3 (\circ) or 6 mM ATP (\bullet); 6 mM ATP + 0.5 (\square) or 2 mM Mg^{2+} (\blacksquare). K_i and K'_i values were obtained as detailed in the Kinetic analyses section. Each point represents the mean \pm SD from three experiments on distinct mitochondrial preparations. Different letters indicate significant differences ($P \leq 0.05$).

1
2
3
4
5
6
7
8
9
10
11
12
13
14
15
16
17
18
19
20
21
22
23
24
25
26
27
28
29
30
31
32
33
34
35
36
37
38
39
40
41
42
43
44
45
46
47
48
49
50
51
52
53
54
55
56
57
58
59
60

Figure 6. Features of the purified F_1 domain and F-ATPase responses to inhibitors (Is- F_1). A) Upper panel: the (I), (II) and (III) SDS–PAGE lanes are biological replicates of purified F_1 domain. On the left-hand lane, broad-range molecular mass marker. On the right-hand side the F_1 subunit migration positions are indicated. Lower panel: the catalytic β subunit band identified by Western Blot assay. The Ca^{2+} - (B) and Mg^{2+} -dependent (C) F_1 -ATPase activities were evaluated in the absence and in the presence of the inhibitors: 3 μ g/mL oligomycin; 75 μ M NBD-Cl; 204 μ M piceatannol; 0.8 mM resveratrol; 0.75 mM quercetin. Each value represents the mean \pm SD from three independent experiments carried out on distinct F_1 preparations. The asterisk (*) indicates significantly different enzyme activity values ($P \leq 0.05$) in the absence and in the presence of inhibitors.

Figure 7. Evaluation of PTP opening. Representative curves (A) of the calcium retention capacity (CRC) and (B) of the membrane potential ($\Delta\phi$) in mitochondrial preparations. CRC and $\Delta\phi$ were monitored in response to subsequent 20 μ M $CaCl_2$ pulses (shown by the arrows), as detailed in the Methods Section, in the absence (Control) and in the presence of the inhibitors 1 μ M CsA, 4 μ M NBD-Cl, 80 μ M piceatannol, 30 μ M resveratrol, 200 μ M quercetin.

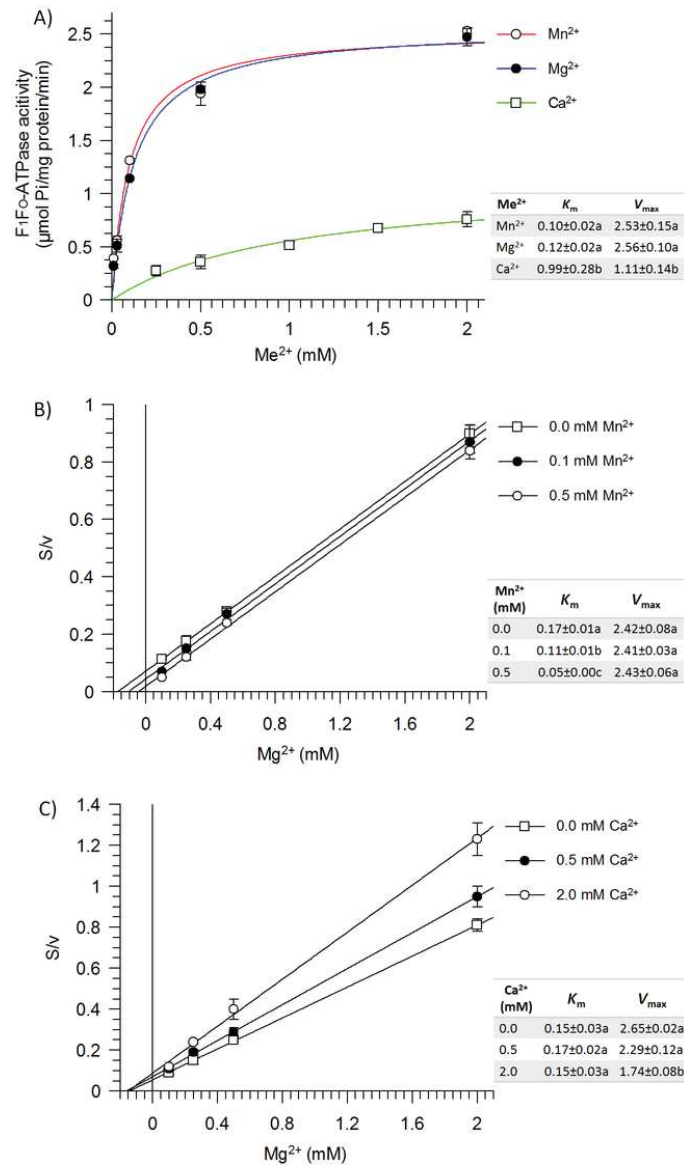


Figure 1. Mitochondrial F1FO-ATPase activities activated by divalent cations. A) Michealis-Menten plot of ATP hydrolysis sustained by Mn²⁺, Mg²⁺ or Ca²⁺. Hanes plots of the Mg²⁺-activated F1FO-ATPase activity in the absence (□) or in the presence of 0.1 mM (●) and 0.5 mM (○) Mn²⁺ (B); in the absence (□) or in presence of 0.5 mM (●) and 2.0 mM (○) Ca²⁺ (C). Km and Vmax are expressed in mM and μmol Pi·mg protein⁻¹·min⁻¹, respectively. Data represent the mean ± SD from three independent experiments carried out on distinct mitochondrial preparations. Different letters indicate significantly different values within each treatment (P ≤ 0.05).

55x95mm (300 x 300 DPI)

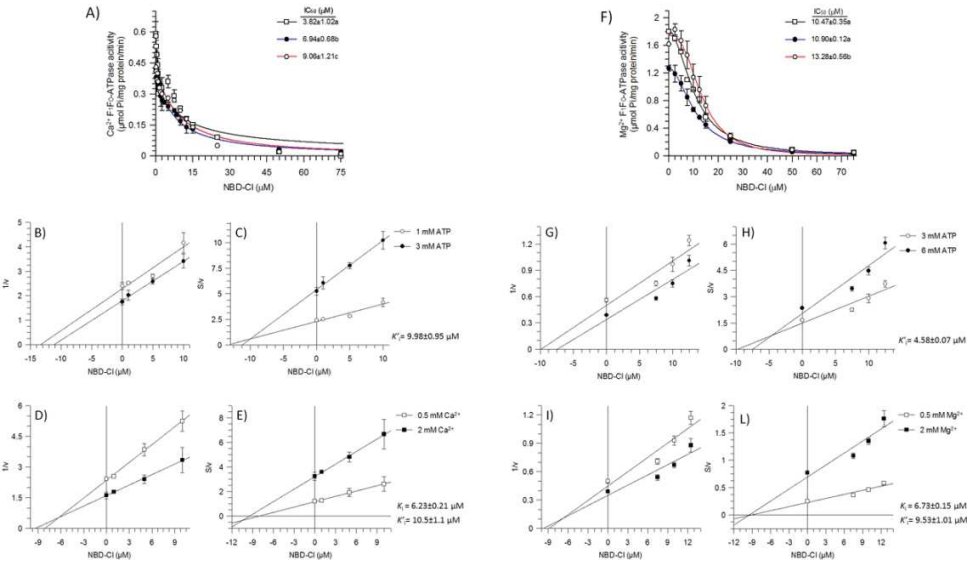


Figure 2. NBD-Cl inhibition on the Ca²⁺- (A-E) and Mg²⁺-activated (F-L) F1FO-ATPases. A) Dose-response curve at: 3 mM ATP + 2 (□) or 0.5 mM Ca²⁺ (●); 1 mM ATP + 2 mM Ca²⁺ (○). Dixon (B, D) and Cornish-Bowden (C, E) plots at 2 mM Ca²⁺ + 1 (○) or 3 mM ATP (●); 3 mM ATP + 0.5 (□) or 2 mM (■) Ca²⁺. (F) Dose-response curve at: 6 mM ATP + 2 (□) or 0.5 mM Mg²⁺ (●); 3 mM ATP + 2 mM Mg²⁺ (○). Dixon (G, I) and Cornish-Bowden (H; L) plots at 2 mM Mg²⁺ + 3 (○) or 6 mM ATP (●); 6 mM ATP + 0.5 (□) or 2 mM Mg²⁺ (■). K_i and K_i' values were obtained as detailed in the Kinetic analyses section. Each point represents the mean ± SD from three experiments on distinct mitochondrial preparations. Different letters indicate significant differences (P ≤ 0.05).

107x62mm (300 x 300 DPI)

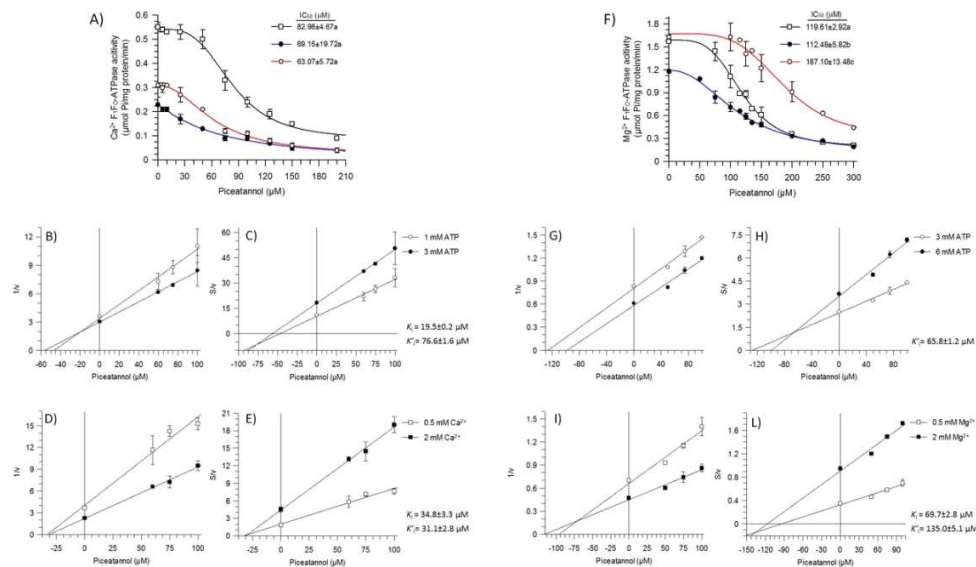


Figure 3. Piceatannol inhibition on the Ca²⁺- (A-E) and Mg²⁺-activated (F-L) F1FO-ATPases. A) Dose-response curve at: 3 mM ATP + 2 mM Ca²⁺ (□) or 0.5 mM Ca²⁺ (●); 1 mM ATP + 2 mM Ca²⁺ (○). Dixon (B, D) and Cornish-Bowden (C, E) plots at 2 mM Ca²⁺ + 1 mM ATP (○) or 3 mM ATP (●); 3 mM ATP + 0.5 mM Ca²⁺ (□) or 2 mM Ca²⁺ (■). (F) Dose-response curve at: 6 mM ATP + 2 mM Mg²⁺ (□) or 0.5 mM Mg²⁺ (●); 3 mM ATP + 2 mM Mg²⁺ (○). Dixon (G, I) and Cornish-Bowden (H, L) plots at 2 mM Mg²⁺ + 3 mM ATP (○) or 6 mM ATP (●); 6 mM ATP + 0.5 mM Mg²⁺ (□) or 2 mM Mg²⁺ (■). K_i and K_i' values were obtained as detailed in the Kinetic analyses section. Each point represents the mean ± SD from three experiments on distinct mitochondrial preparations. Different letters indicate significant differences (P ≤ 0.05).

107x62mm (300 x 300 DPI)

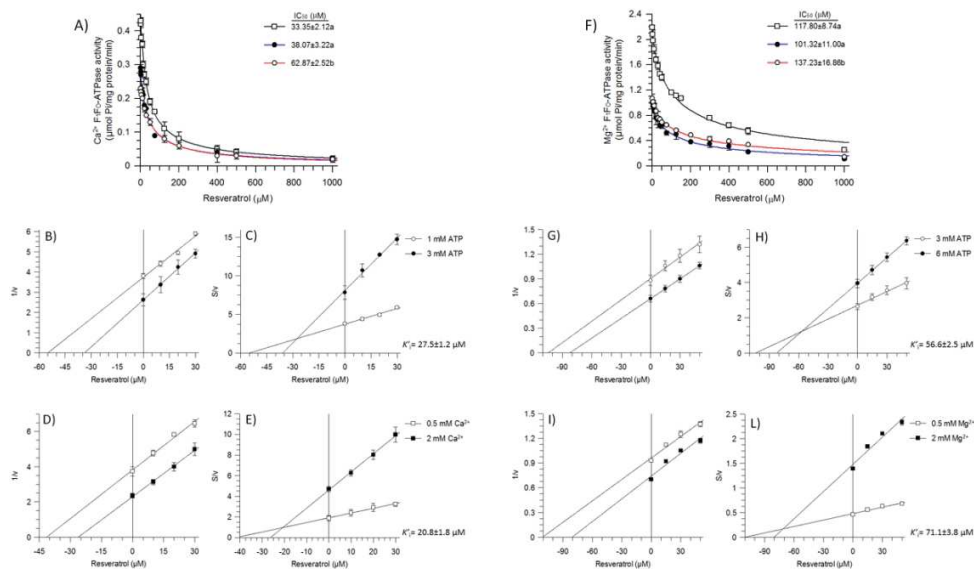


Figure 4. Resveratrol inhibition on the Ca^{2+} - (A-E) and Mg^{2+} -activated (F-L) F_1F_0 -ATPases. A) Dose-response curve at: 3 mM ATP + 2 (□) or 0.5 mM Ca^{2+} (●); 1 mM ATP + 2 mM Ca^{2+} (○). Dixon (B, D) and Cornish-Bowden (C, E) plots at 2 mM Ca^{2+} + 1 (○) or 3 mM ATP (●); 3 mM ATP + 0.5 (□) or 2 mM (■) Ca^{2+} . (F) Dose-response curve at: 6 mM ATP + 2 (□) or 0.5 mM Mg^{2+} (●); 3 mM ATP + 2 mM Mg^{2+} (○). Dixon (G, I) and Cornish-Bowden (H; L) plots at 2 mM Mg^{2+} + 3 (○) or 6 mM ATP (●); 6 mM ATP + 0.5 (□) or 2 mM Mg^{2+} (■). K_i and K_i' values were obtained as detailed in the Kinetic analyses section. Each point represents the mean \pm SD from three experiments on distinct mitochondrial preparations. Different letters indicate significant differences ($P \leq 0.05$).

106x61mm (300 x 300 DPI)

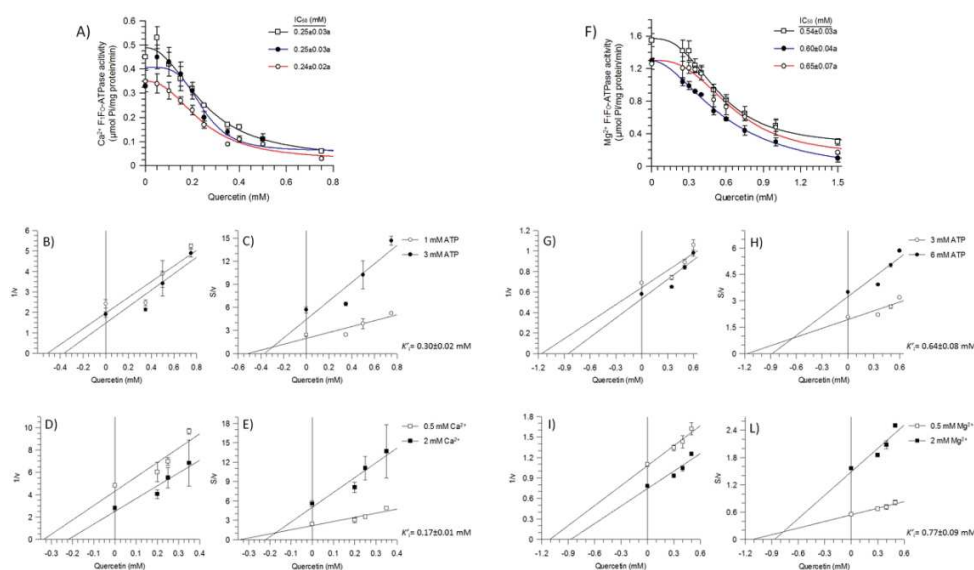


Figure 5. Quercetin inhibition on the Ca^{2+} - (A-E) and Mg^{2+} -activated (F-L) F1FO-ATPases. A) Dose-response curve at: 3 mM ATP + 2 mM Ca^{2+} (□) or 0.5 mM Ca^{2+} (●); 1 mM ATP + 2 mM Ca^{2+} (○). Dixon (B, D) and Cornish-Bowden (C, E) plots at 2 mM Ca^{2+} + 1 mM ATP (○) or 3 mM ATP (●); 3 mM ATP + 0.5 mM Ca^{2+} (□) or 2 mM Ca^{2+} (■). (F) Dose-response curve at: 6 mM ATP + 2 mM Mg^{2+} (□) or 0.5 mM Mg^{2+} (●); 3 mM ATP + 2 mM Mg^{2+} (○). Dixon (G, I) and Cornish-Bowden (H, L) plots at 2 mM Mg^{2+} + 3 mM ATP (○) or 6 mM ATP (●); 6 mM ATP + 0.5 mM Mg^{2+} (□) or 2 mM Mg^{2+} (■). K_i and K_i' values were obtained as detailed in the Kinetic analyses section. Each point represents the mean \pm SD from three experiments on distinct mitochondrial preparations. Different letters indicate significant differences ($P \leq 0.05$).

107x61mm (300 x 300 DPI)

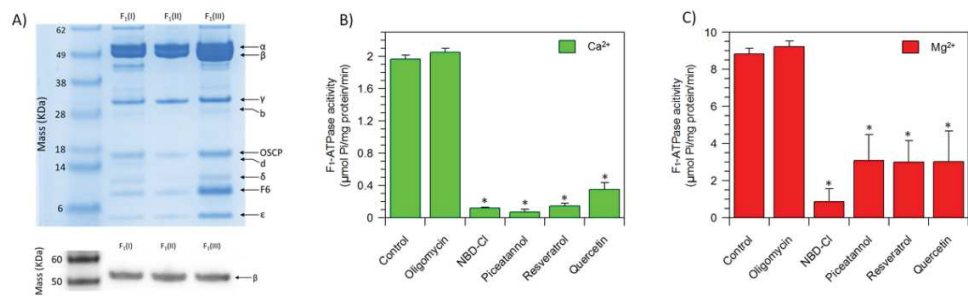


Figure 6. Features of the purified F1 domain and F-ATPase responses to inhibitors (Is-F1). A) Upper panel: the (I), (II) and (III) SDS-PAGE lanes are biological replicates of purified F1 domain. On the left-hand lane, broad-range molecular mass marker. On the right-hand side the F1 subunit migration positions are indicated. Lower panel: the catalytic β subunit band identified by Western Blot assay. The Ca²⁺- (B) and Mg²⁺-dependent (C) F1-ATPase activities were evaluated in the absence and in the presence of the inhibitors: 3 μ g/mL oligomycin; 75 μ M NBD-Cl; 204 μ M piceatannol; 0.8 mM resveratrol; 0.75 mM quercetin. Each value represents the mean \pm SD from three independent experiments carried out on distinct F1 preparations. The asterisk (*) indicates significantly different enzyme activity values ($P \leq 0.05$) in the absence and in the presence of inhibitors.

102x31mm (300 x 300 DPI)

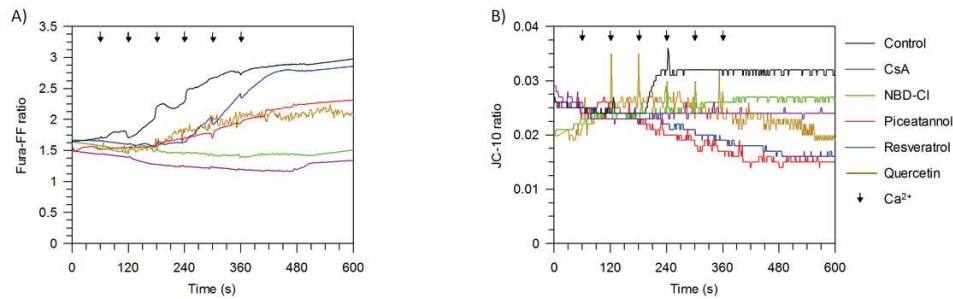


Figure 7. Evaluation of PTP opening. Representative curves (A) of the calcium retention capacity (CRC) and (B) of the membrane potential ($\Delta\psi$) in mitochondrial preparations. CRC and $\Delta\psi$ were monitored in response to subsequent 20 μM CaCl_2 pulses (shown by the arrows), as detailed in the Methods Section, in the absence (Control) and in the presence of the inhibitors 1 μM CsA, 4 μM NBD-Cl, 80 μM piceatannol, 30 μM resveratrol, 200 μM quercetin.

96x29mm (300 x 300 DPI)

1
2
3
4
5
6
7
8
9
10
11
12
13
14
15
16
17
18
19
20
21
22
23
24
25
26
27
28
29
30
31
32
33
34
35
36
37
38
39
40
41
42
43
44
45
46
47
48
49
50
51
52
53
54
55
56
57
58
59
60

Figure S1

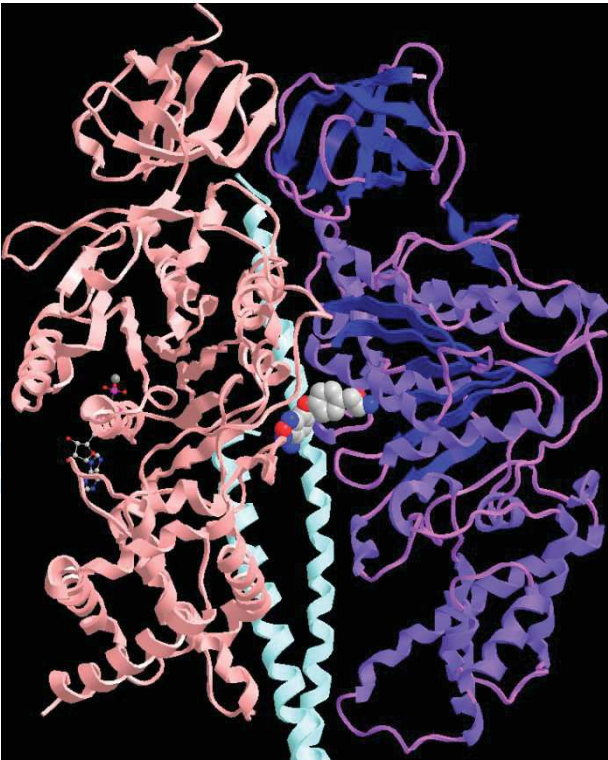


Fig. S1. Representation of α_E - β_E structure of F_1 -ATPase covalently inhibited with NBD. The α_E subunit in salmon color with the MgATP molecule in ball and stick bound to non-catalytic site of subunit. The β_E subunit in violet with NBD in space filling mode covalent bond to subunit. The γ subunit is in light blue color. Protein subunits are drawn as ribbon representations (modified PDB ID codes: 1NBM).

Figure S2

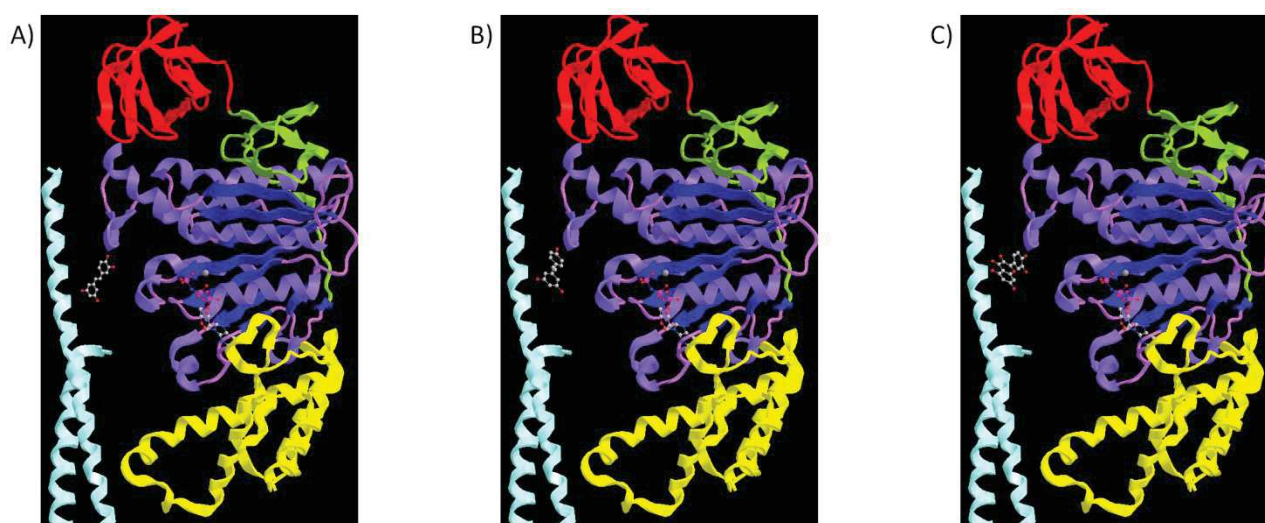


Fig. S2. Representation of polyphenolic phytochemical molecules bound on γ - β_{TP} structure of F₁-ATPase. The γ subunit is in light blue color, while in the β_{TP} subunit has the "crown region" (top) in red, the "long connecting loop" in olive, the "nucleotide-binding domain" (middle) in violet and the C-terminal domain (bottom) in yellow. The MgATP molecule in ball and stick is bound to β_{TP} subunit. Piceatannol (A), resveratrol (B) and quercetin (C) in ball and stick are bound between the C-terminal tip of the γ subunit and the "bearing" consisting of the hydrophobic annular sleeve provided by the loop region below the "crown region" of β and α subunit. For clarity, the three α subunits and the β_E and β_{DP} subunits have been removed. Protein subunits are drawn as ribbon representations (modified PDB ID codes: 2JIZ).

Figure S3

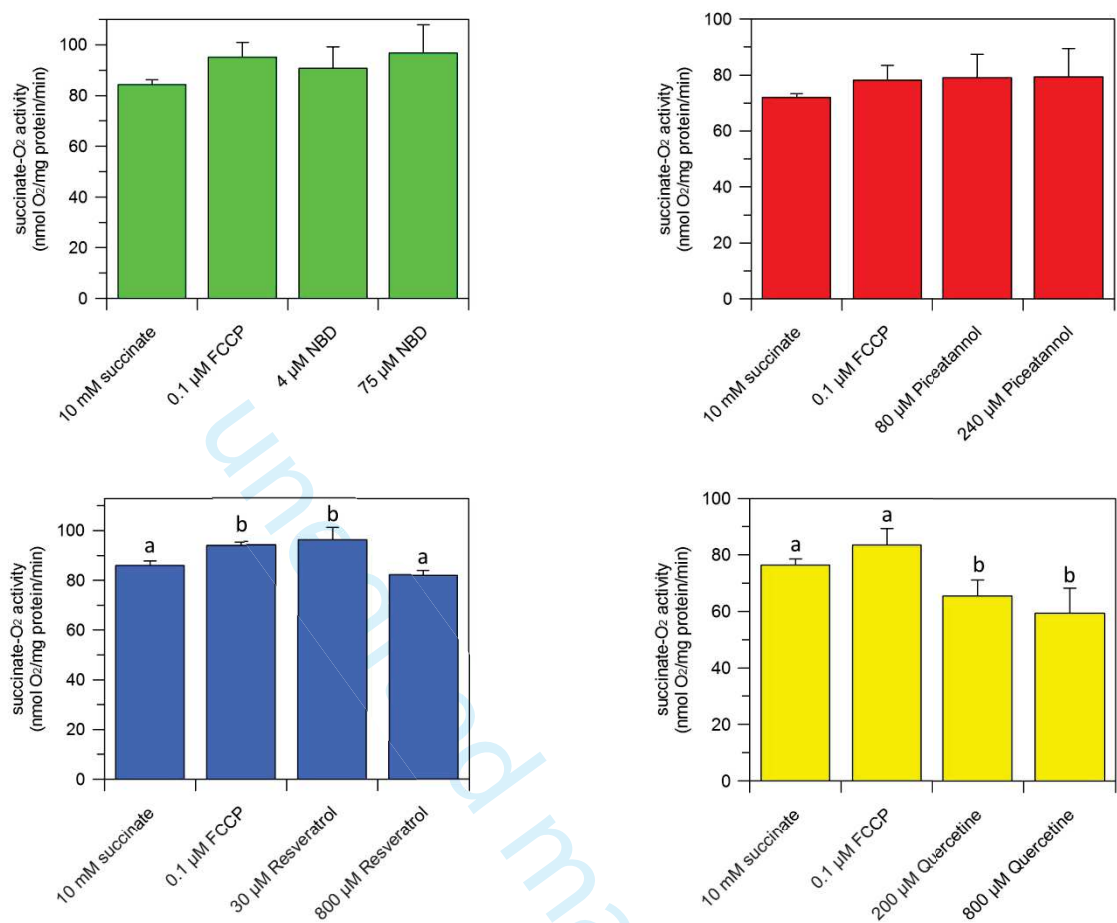


Fig. S3. Is-F₁ effect on mitochondrial succinate-O₂ oxidase activity. Data represent the mean ± SD (vertical bars) of at least three experiments carried out on distinct mitochondrial preparations. In each panel different letters indicate significantly different values within each treatment ($P \leq 0.05$).